Metadata of the chapter that will be visualized online SAND2015-1228C

Chapter Title	Considerations for Indirect Parameter Estimation in Nonlinear Reduced Order Models	
Copyright Year	2015	
Copyright Holder	Springer International Publishing Switzerland	
Corresponding Author	Family Name	**Guerin**
	Particle	
	Given Name	**Lorraine C. M.**
	Suffix	
	Division	Department of Engineering Physics
	Organization	University of Wisconsin
	Address	Madison, WI 53706, USA
	Email	lguerin@wisc.edu
Author	Family Name	**Kuether**
	Particle	
	Given Name	**Robert J.**
	Suffix	
	Division	Department of Engineering Physics
	Organization	University of Wisconsin
	Address	Madison, WI 53706, USA
	Email	rkuether@wisc.edu
Author	Family Name	**Allen**
	Particle	
	Given Name	**Matthew S.**
	Suffix	
	Division	Department of Engineering Physics
	Organization	University of Wisconsin
	Address	Madison, WI 53706, USA
	Email	msallen@engr.wisc.edu
Abstract	Over the past few decades, there have been many developments in techniques that extract a reduced order model (ROM) from a geometrically nonlinear finite element model. The enforced displacement ROM strategy that is of interest in this work is known as an indirect approach because it does not require altering the finite element code. Instead, one uses a series of static displacement fields applied to the nonlinear finite element model to estimate the nonlinear stiffness coefficients in the reduced equations. Geometric nonlinearity causes the bending and membrane displacements to become coupled, and the enforced displacements method requires that the kinematics of the membrane motion be explicitly included in the basis using either	

axial vibration modes or dual modes. This work explores the accuracy of the enforced displacements ROM strategy by comparing the efficiency of these basis vectors, as well as the use of three different parameter estimation procedures and the effect of scaling factors on the static load cases used to generate the ROM. The different modeling decisions are shown to have a very significant effect on the accuracy of the ROMs, and the comparisons are used to suggest best practices that result in the most accurate ROMs. These issues are explored using finite element models of a flat geometrically nonlinear beam with fixed-fixed boundary conditions and a flat geometrically nonlinear exhaust cover plate. The effect of each of the modeling decisions on the resulting enforced displacement ROM is evaluated by computing the Nonlinear Normal Modes (NNMs) of the full finite element model and comparing them with the NNMs calculated from the ROMs. The NNMs offer a powerful metric that indicates whether or not the ROM captures a variety of important physics in the original model.

Keywords (separated by "-")	Reduced order modeling - Geometric nonlinearity - Nonlinear dynamics - Nonlinear normal modes - Finite element analysis

Chapter 30
Considerations for Indirect Parameter Estimation in Nonlinear Reduced Order Models

Lorraine C.M. Guerin, Robert J. Kuether, and Matthew S. Allen

Abstract Over the past few decades, there have been many developments in techniques that extract a reduced order model (ROM) from a geometrically nonlinear finite element model. The enforced displacement ROM strategy that is of interest in this work is known as an indirect approach because it does not require altering the finite element code. Instead, one uses a series of static displacement fields applied to the nonlinear finite element model to estimate the nonlinear stiffness coefficients in the reduced equations. Geometric nonlinearity causes the bending and membrane displacements to become coupled, and the enforced displacements method requires that the kinematics of the membrane motion be explicitly included in the basis using either axial vibration modes or dual modes. This work explores the accuracy of the enforced displacements ROM strategy by comparing the efficiency of these basis vectors, as well as the use of three different parameter estimation procedures and the effect of scaling factors on the static load cases used to generate the ROM. The different modeling decisions are shown to have a very significant effect on the accuracy of the ROMs, and the comparisons are used to suggest best practices that result in the most accurate ROMs. These issues are explored using finite element models of a flat geometrically nonlinear beam with fixed-fixed boundary conditions and a flat geometrically nonlinear exhaust cover plate. The effect of each of the modeling decisions on the resulting enforced displacement ROM is evaluated by computing the Nonlinear Normal Modes (NNMs) of the full finite element model and comparing them with the NNMs calculated from the ROMs. The NNMs offer a powerful metric that indicates whether or not the ROM captures a variety of important physics in the original model.

Keywords Reduced order modeling • Geometric nonlinearity • Nonlinear dynamics • Nonlinear normal modes • Finite element analysis

30.1 Introduction

One popular modeling approach in structural dynamics uses finite element analysis (FEA) to generate the discretized equations of motion. Detailed meshes may be needed to capture precise geometric features of a realistic structure, for example, the stiffeners in an aircraft panel, so a large number of degrees-of-freedom (DOF) may be needed to accurately describe the motion. Furthermore, when the model exhibits large deformations, the equations of motion become nonlinear and the computational cost increases dramatically. As a result, many efforts have been put forth over the last few decades to develop reduced order modeling strategies for geometrically nonlinear FEA models [1, 2]. One class of reduction methods, referred to as *indirect* methods, uses a Galerkin approach to reduce the equations using a smaller set of modal DOF. An additional nonlinear term persists in the modal equations due to the geometric nonlinearity, whose coefficients are determined through a series of static load cases. This paper explores some of the challenges with producing accurate nonlinear reduced order models (ROMs) using the enforced displacement procedure [3], particularly issues related to mode selection, parameter estimation and displacement scaling factors.

The enforced displacement procedure was first developed by Muravyov and Rizzi in [3]. A set of component modes describe the kinematics of a geometrically nonlinear FEA model, and are used to reduce the full model down to a low order set of modal equations. These equations have a linear modal mass and modal stiffness term that can be determined analytically since one typically has access to the linear mass and stiffness matrices in a commercial FEA package. However, the nonlinear terms are usually not available unless one has access to the internals of the software. Assuming that the material is linear elastic, and a quadratic strain–displacement relation is used, the nonlinear restoring force in modal form is a quadratic

L.C.M. Guerin (✉) • R.J. Kuether • M.S. Allen
Department of Engineering Physics, University of Wisconsin, Madison, WI 53706, USA
e-mail: lguerin@wisc.edu; rkuether@wisc.edu; msallen@engr.wisc.edu

G. Kerschen (ed.), *Nonlinear Dynamics, Volume 1*, Conference Proceedings of the Society for Experimental Mechanics Series, DOI 10.1007/978-3-319-15221-9_30

and cubic polynomial function of the modal displacements with unknown stiffness coefficients. To determine these values, the nonlinear FEA model is enforced to take the shape of the scaled component mode shapes, or a combination of these shapes, and a static analysis is performed to solve for the reactions forces to hold each shape. The nonlinear stiffness terms in the modal equations are determined using a series of these displacements and reaction forces.

The bending-membrane coupling must be accounted for explicitly when creating ROMs using the enforced displacement procedure. As the model experiences large bending deflections, membrane stretching can occur, so both bending and membrane type component modes are explicitly needed in the basis set. This paper explores two approaches to capture these kinematics, namely the use of axial vibration modes, and the dual modes method in [4]. Another modeling consideration is the procedure used to fit the nonlinear stiffness coefficients based on a series of static solutions. The method referred to as RANSTEP throughout this paper, which was first introduced in [3], uses special combinations of modal displacements to solve for a small number of coefficients at a time. The coefficients could also be found by setting up a least squares problem involving all of the static load solutions [5]. Finally, the effect of scaling on the static displacement fields is explored in this paper using the constant modal scaling (CS) method proposed originally in [3] along with the constant modal displacement (CD) approach used in [6–8]. The results presented here will show that the resulting accuracy of the ROM equations greatly depends on the procedures used to fit the nonlinear stiffness coefficients and capture the membrane motions.

Rizzi and Przekop explored the effect of basis selection on the resulting ROM equations in [9], and assessed the accuracy of the ROM by comparing its response to random inputs with the response of the full-order model (which is quite expensive to compute). The authors recently suggested that a more rigorous comparison between two ROMs could be made by comparing their nonlinear normal modes and used this to compare two ROM procedures [6]. The nonlinear normal mode [10, 11], which is defined as a *not necessarily synchronous periodic response of the undamped nonlinear equations of motion,* provides an excellent metric for comparison between ROMs and the full FEA model since these solutions are independent of any external forces, and capture a wide range of response amplitudes seen by the nonlinear system. Previous works have shown that if the NNMs predicted by the ROM converge, then the response predictions also tend to be accurate [12, 13]. The work presented in this paper is an extension of the work in [6], but here we only focus on variations on the enforced displacement procedure. The effect of mode selection, methods to identify the nonlinear stiffness terms, and the scaling on the static load cases are all explored simultaneously to attempt to determine the best practices when using the enforced displacements ROM approach.

The paper is organized as follows. Section 30.2 reviews the theory of the enforced displacement reduction strategy, along with considerations for mode selection, scaling of the static load cases, and identification of nonlinear stiffness terms. The results in Sects. 30.3 and 30.4 demonstrate the reduction strategy applied to a geometrically nonlinear flat beam with clamped-clamped boundary conditions. The nonlinear normal modes are used to compare a set of ROM equations generated with different variations on the enforced displacements procedure, showing that the ROM predictions can diverge from those predicted by the full FEA model in certain cases. Section 30.5 presents the results from a more complicated model of an exhaust cover plate with geometric nonlinearity, using the best practices learned from the beam model. Section 30.6 presents the conclusions.

30.2 Theoretical Development

The equations of motion for a geometrically nonlinear, N degree-of-freedom (DOF) system, discretized by the finite element method can be written as

$$\mathbf{M}\ddot{\mathbf{x}}(t) + \mathbf{K}\mathbf{x}(t) + \mathbf{f}_{NL}(\mathbf{x}) = \mathbf{f}(t) \tag{30.1}$$

where $\mathbf{M}$ and $\mathbf{K}$ are the $N \times N$ mass and stiffness matrices, respectively and the $N \times 1$ displacement and acceleration vectors are respectively represented as $\mathbf{x}(t)$ and $\ddot{\mathbf{x}}(t)$. The $N \times 1$ external force vector is denoted as $\mathbf{f}(t)$, while $\mathbf{f}_{NL}(\mathbf{x})$ is the $N \times 1$ nonlinear restoring force vector due to the geometric nonlinearity.

The size of the equations of motion are reduced using a coordinate transformation based on a set of component modes. The relationship between physical and generalized coordinates is described as

$$\mathbf{x}(t) = \mathbf{T}\mathbf{q}(t) \tag{30.2}$$

where $\mathbf{q}(t)$ is the $m \times 1$ time-dependent modal displacement vector and $\mathbf{T}$ is the $N \times m$ matrix of component modes. A subset of m basis vectors are included in each column of $\mathbf{T}$, such that the degrees-of-freedom are significantly reduced ($m << N$). By substituting Eq. (30.2) into Eq. (30.1), and pre-multiplying by $\mathbf{T}^{\mathbf{T}}$, the reduced equations of motion become

$$\widehat{\mathbf{M}}\ddot{\mathbf{q}} + \widehat{\mathbf{K}}\mathbf{q} + \mathbf{T}^{\mathrm{T}}\mathbf{f}_{NL}\left(\mathbf{Tq}\right) = \mathbf{T}^{\mathrm{T}}\mathbf{f}(t) \tag{30.3}$$

$$\widehat{\mathbf{M}} = \mathbf{T}^{\mathrm{T}}\mathbf{MT} \tag{30.4}$$

$$\widehat{\mathbf{K}} = \mathbf{T}^{\mathrm{T}}\mathbf{KT} \tag{30.5}$$

The $()^{\mathrm{T}}$ operator represents the transpose operator. The nonlinear restoring force in the modal form of the equation can be generalized as

$$\mathbf{T}^{\mathrm{T}}\mathbf{f}_{NL}\left(\mathbf{Tq}\right) = \boldsymbol{\theta}(\mathbf{q}) \tag{30.6}$$

which is a nonlinear function of each of the displacements in $\mathbf{q}$. For linear elastic materials with quadratic strain–displacement relationships, it has been shown in previous works [1, 2] that the r^{th} nonlinear restoring force in modal form may be written as

$$\theta_r\left(q_1, q_2, \ldots, q_m\right) = \sum_{i=1}^{m}\sum_{j=i}^{m} B_r\left(i, j\right) q_i q_j + \sum_{i=1}^{m}\sum_{j=i}^{m}\sum_{k=j}^{m} A_r\left(i, j, k\right) q_i q_j q_k$$
$$r = 1, 2, \ldots, m \tag{30.7}$$

where B_r are the quadratic nonlinear stiffness coefficients and A_r are the cubic nonlinear stiffness coefficients for the r^{th} nonlinear modal equation. Within most commercial finite element packages, the nonlinear stiffness matrices are inaccessible, and therefore they must be determined indirectly by applying a set of forces or displacements to the FEA model.

There are several methods to evaluate the nonlinear stiffness coefficients. In this paper, the enforced displacement (ED) procedure is used exclusively. The ED process uses specific static displacements fields (i.e. linear combinations of the component modes in $\mathbf{T}$) that are enforced on the model using any suitable commercial FEA solver. For example, the c^{th} static displacement can be a combination of up to three component modes given as

$$\mathbf{x}_c = \mathbf{T}_i\widehat{q}_i + \mathbf{T}_j\widehat{q}_j + \mathbf{T}_k\widehat{q}_k \tag{30.8}$$

where the $N \times 1$ vector $\mathbf{x}_c$ is an enforced displacement for the c^{th} static load case, and each component mode denoted with subscript i, j, or k is scaled with the scalar amplitude $\widehat{q}$. The FEA software computes the reaction force, $\mathbf{f}_{T,c}$, necessary to hold the displacement field $\mathbf{x}_{\mathrm{c}}$, which can be broken into linear and nonlinear internal force components by the relation

$$\mathbf{f}_{T,c} = \mathbf{f}_L + \mathbf{f}_{NL} = \mathbf{K}\mathbf{x}_c + \mathbf{f}_{NL}\left(\mathbf{x}_c\right) \tag{30.9}$$

After computing the nonlinear reaction force $\mathbf{f}_{T,c}$, a series of these displacement and forces can be used to determine the nonlinear stiffness coefficients in Eq. (30.7), as will be reviewed in Sect. 30.2.3.

30.2.1 Selection of Modes

Mode selection becomes particularly important for finite element models with geometric nonlinearity. It is common to use the linearized, mass normalized vibration modes φ_r as basis vectors, which are computed from the eigenvalue problem $\left(\mathbf{K} - \omega_r^2\mathbf{M}\right)\boldsymbol{\varphi}_r = \mathbf{0}$. It is important to explicitly include the appropriate bending and membrane modes for the reduction basis of the ED procedure in order to capture the kinematics of this bending-membrane coupling. The higher frequency membrane motions can be incorporated into the basis by either including axial vibration modes, or using an alternative set of component modes referred to as dual modes. Guidance for the computation and selection of each type of membrane mode is provided below.

30.2.1.1 Axial Vibration Modes

Many works have used axial modes to capture the membrane effects [1, 6, 9, 14] for enforced displacement ROMs. Since these membrane motions are typically driven by large deformations of the bending modes, a set of these axial modes can be selected and augmented to each bending mode in the basis set as done in [6]. The augmented axial vibration modes for the r^{th} bending mode are determined by applying a force proportional to that bending mode shape to the finite element model as

$$\mathbf{K}\mathbf{x} + \mathbf{f}_{NL}(\mathbf{x}) = \mathbf{M}\boldsymbol{\varphi}_r \widehat{f}_r \tag{30.10}$$

The force amplitude $\widehat{f}_r$ should be large enough to excite the nonlinearity in the response such that the displacements contain components of the r^{th} bending mode as well as components of other modes that are statically coupled to that mode. The static displacement is then projected onto all the linear, mass normalized modes as $\mathbf{q} = \boldsymbol{\Phi}^{\mathrm{T}}\mathbf{M}\mathbf{x}$, and axial modes with the largest contribution to the response should be selected as the axial basis augmented to the r^{th} bending mode. For flat structures, the distinction for axial and bending type motion is clear. However, curved structures tend to produce vibrations modes that are coupled between transverse and in-plane deformations making it more difficult to distinguish between the two. This approach is discussed in more detail in [6].

30.2.1.2 Dual Modes

A systematic approach to generating the membrane basis was developed by Kim et al. using the concept of the dual mode [4]. The dual modes are computed from a pre-selected set of bending mode shapes using static forces applied to the nonlinear structure. There are three types of dual modes, which are referred to as first, second, and third generation dual modes. For the first generation dual mode, a static force proportional to only one bending mode is applied to the FEA model, given as

$$\mathbf{f}_T = \mathbf{M}\boldsymbol{\varphi}_r \widehat{f}_r \tag{30.11}$$

Again, $\widehat{f}_r$ is the scaling value on the applied force that sufficiently excites a nonlinear response. Using a commercial finite element package, the resulting static displacement field is computed as $\mathbf{u}_r$. The residual component of the response, that which remains after removing the component of the r^{th} bending mode φ_r, is isolated by the following relationship

$$\mathbf{v}_r^{(1)} = \mathbf{u}_r - \boldsymbol{\varphi}_r^T \mathbf{M}\mathbf{u}_r \boldsymbol{\varphi}_r \tag{30.12}$$

where $\mathbf{v}_r$ represents the remaining displacement field. This field contains the membrane motion due to bending displacement in the r^{th} mode. The notation $^{(1)}$ denotes that this type of response is used to compute a first generation the dual mode. A set of first generation dual modes are computed for all bending modes in the basis set.

Similarly, second generation dual modes result from an applied static force that is a linear combination of two bending mode shapes, such as

$$\mathbf{f}_T = \mathbf{M}\boldsymbol{\varphi}_i \widehat{f}_i + \mathbf{M}\boldsymbol{\varphi}_j \widehat{f}_j \tag{30.13}$$

The linear bending modes components are subtracted from the resultant displacement field as given below

$$\mathbf{v}_{ij}^{(2)} = \mathbf{u}_{ij} - \boldsymbol{\varphi}_i^T \mathbf{M}\mathbf{u}_{ij} \boldsymbol{\varphi}_i - \boldsymbol{\varphi}_j^T \mathbf{M}\mathbf{u}_{ij} \boldsymbol{\varphi}_j \tag{30.14}$$

Third generation dual modes are found by applying forces made up of linear combinations of three bending modes.

The final computational step for the dual modes basis is to make the dual modes mutually orthonormal with respect to the linear modes and the mass matrix. Each dual mode is orthonormalized with respect to the mass matrix using a Gram-Schmidt procedure, so the final orthonormal basis vectors $\boldsymbol{\Xi}_{ijk}^{(g)}$ are found using the following.

$$\boldsymbol{\Xi}_{ijk}^{(g)} = \mathbf{v}_{ijk}^{(g)} - \sum_{l=1}^{p} \boldsymbol{\varphi}_l \boldsymbol{\varphi}_l^T \mathbf{M}\mathbf{v}_{ijk}^{(g)} \tag{30.15}$$

The subscripts *i, j,* and *k* represent the linear mode(s) used to generate the dual mode, superscript *g* represents the type of dual mode (first, second, or third generation), and *p* represents the number of linear bending modes in the basis. For further details, see [4].

30.2.2 Scaling of Modes

Two scaling methods are used in this paper when determining the displacement magnitude $\widehat{q}$ of each component mode in Eq. (30.8). The displacement level dictates the level of nonlinearity excited during the static load cases used to fit the nonlinear stiffness coefficients. The two scaling approaches are the constant modal scaling (CS) method and the constant modal displacement (CD) method. Using the CD approach from [6], a scaling value $\widehat{q}_r$ for the r^{th} modal displacement is defined as

$$\widehat{q}_r = CD_r = \frac{w_{\max,r}}{\max\limits_{d}(\mathbf{T}_r)} \tag{30.16}$$

where $w_{\max,r}$ is the desired maximum displacement in physical coordinates for the r^{th} mode, and $\max\limits_{d}(\mathbf{T}_r)$ is the maximum displacement (i.e. ignoring any rotations) in the r^{th} component mode shape. The CD method sets a specific scaling factor for each mode in the displacement fields generated by Eq. (30.8). The authors have found that it is important to determine adequate scaling levels for the bending and membrane modes in order to obtain accurate ROM equations. One approach to guide the range of appropriate scaling values is to create a set of single-mode ROMs, which ultimately have one quadratic and one cubic nonlinear stiffness term. By tracking the nonlinear stiffness coefficients as a function of the maximum displacement, $w_{\max,r}$, the coefficients should converge around a range of scaling levels, indicating that the geometric nonlinearity is sufficiently exercised.

Previous works on the enforced displacement procedure have used what is referred to here as the CS approach, as recommended in [3]. The CS factor takes the CD scaling factor for the lowest frequency mode in the basis set in Eq. (30.16), and uses the same scaling factor for all modes in the basis set as $\widehat{q}_r = \text{CD}_1$. The scaling factor is chosen based on the maximum displacement of the first bending mode included in the ROM, allowing for no control over the displacement level of the other modes in the basis. Displacements on the order of the thickness of the structure are recommended in [3], however the results in Sect. 30.3 show that this approach may not always produce the most accurate model.

Mignolet, Perez, Wang and others have also employed the enforced displacements procedure successfully to many structures [2, 7, 8, 15]. They typically set CD_r for each mode such that each bending mode displaces 1.0 times the thickness and a displacement < 1.0 times the thickness for the axial or dual modes. The optimal CD values are problem dependent and so they typically employ a few values near 1.0 thickness and check whether the ROM coefficients vary significantly. They also typically use the cleaning procedure described in [15] to set to zero any cubic $\text{A}_r(r, r, r)$ and quadratic $\text{B}_r(r, r)$ terms involving only one axial (or dual) mode. Finally, it should be noted that their approach to determine the ROM coefficients differs slightly from that outlined in Sect. 30.2.3.3 in that they estimate both the linear and nonlinear terms in the ROM from the results of the static load cases. The linear terms can then be compared against the known linear natural frequencies to check the consistency of the results; they may vary from the linear natural frequencies if too large of loads have been applied. This approach was not implemented in this work, but it should be kept in mind as it may explain some of the differences between the scaling values that worked best in this work and those reported in their works.

30.2.3 Identification of Nonlinear Stiffness Coefficients

30.2.3.1 Least Squares Method

The nonlinear stiffness coefficients may be evaluated using the least squares method, which employs a pseudo-inverse of a data matrix to determine the nonlinear stiffness coefficients for the r^{th} modal equation in a single computation. From Eq. (30.6) and a given static solution to the c^{th} load case in Eq. (30.8), the quasi-static modal equations can be rearranged as

$$\sum_{i=1}^{m}\sum_{j=i}^{m} B_r(i,j)\widehat{q}_i\widehat{q}_j + \sum_{i=1}^{m}\sum_{j=i}^{m}\sum_{k=j}^{m} A_r(i,j,k)\widehat{q}_i\widehat{q}_j\widehat{q}_k = \mathbf{T}_r^T\mathbf{f}_{T,c} - \mathbf{T}_r^T\mathbf{K}\mathbf{x}_c \tag{30.17}$$

For P static load cases of different permutations of the mode displacement fields, the relation for the nonlinear stiffness terms for the r^{th} equation can be written generally as

$$\begin{bmatrix} \widehat{q}_1{}^2[1] & \widehat{q}_1\widehat{q}_2[1] & \dots & \widehat{q}_m{}^2[1] & \widehat{q}_1{}^3[1] & \widehat{q}_1{}^2\widehat{q}_2[1] & \dots & \widehat{q}_m{}^3[1] \\ \widehat{q}_1{}^2[2] & \widehat{q}_1\widehat{q}_2[2] & \dots & \widehat{q}_m{}^2[2] & \widehat{q}_1{}^3[2] & \widehat{q}_1{}^2\widehat{q}_2[2] & \dots & \widehat{q}_m{}^3[2] \\ \vdots & \vdots & & \vdots & \vdots & \vdots & & \\ \widehat{q}_1{}^2[P] & \widehat{q}_1\widehat{q}_2[P] & \dots & \widehat{q}_m{}^2[P] & \widehat{q}_1{}^3[P] & \widehat{q}_1{}^2\widehat{q}_2[P] & \dots & \widehat{q}_m{}^3[P] \end{bmatrix} \begin{Bmatrix} B_r(1,1) \\ B_r(1,2) \\ \vdots \\ B_r(m,m) \\ A_r(1,1,1) \\ A_r(1,1,2) \\ \vdots \\ A_r(m,m,m) \end{Bmatrix} = \begin{Bmatrix} \mathbf{T}_r^{\mathrm{T}}\mathbf{f}_{T,1} - \mathbf{T}_r^T\mathbf{K}\mathbf{x}_1 \\ \mathbf{T}_r^{\mathrm{T}}\mathbf{f}_{T,2} - \mathbf{T}_r^T\mathbf{K}\mathbf{x}_2 \\ \vdots \\ \mathbf{T}_r^{\mathrm{T}}\mathbf{f}_{T,P} - \mathbf{T}_r^T\mathbf{K}\mathbf{x}_P \end{Bmatrix} \tag{30.18}$$

Note that each row will contain at most contributions from up to three modes. The algebraic equation in Eq. (30.18) is simplified as

$$\mathbf{G}\boldsymbol{\kappa}_r = \widehat{\mathbf{F}}_r \tag{30.19}$$

where $\mathbf{G}$ represents the data matrix of modal displacements, $\boldsymbol{\kappa}_r$ represents the vector of unknown coefficients for the r^{th} modal equation, and $\widehat{\mathbf{F}}_r$ represents the difference between the modal reaction force and linear contribution of the internal force. The unknown coefficients for the r^{th} modal equations are determined by computing the pseudo-inverse of the data matrix $\mathbf{G}$ in Eq. (30.19). The data matrix is independent of the modal equation being evaluated, so the pseudo-inverse needs to be computed only once. Only the right hand side of Eq. (30.19) need be updated to compute the coefficients for each of the modes described by the subscript r.

30.2.3.2 Least Squares, Constrained Method

The least squares, constrained method evaluates the nonlinear stiffness coefficients with a similar procedure as the least squares method. For multi-mode ROMs, dependency relations between the nonlinear stiffness coefficients are enforced during the fitting procedure. The relations are given as

$$B_k(i,j) = B_i(j,k) = B_j(i,k) \tag{30.20}$$

$$B_i(i,j) = 2B_j(i,i) \tag{30.21}$$

$$A_i(i,i,j) = 3A_j(i,i,i) \tag{30.22}$$

$$A_i(i,j,j) = A_j(i,i,j) \tag{30.23}$$

$$A_l(i,j,k) = A_k(i,j,l) \tag{30.24}$$

$$A_j(i,j,k) = 2A_i(j,j,k) = 2A_k(i,j,j) \tag{30.25}$$

These relations are enforced to ensure that the nonlinear stiffness matrices remain symmetric. The least squares, constrained method must solve for the nonlinear stiffness terms for all of the modal equations with a single pseudo-inverse of a modified data matrix, rather than just the r^{th} equation as done before. This matrix is larger than that in Eq. (30.19). The size of the matrix is not important from the view of computational cost, since the computations in Eqs. (30.18), (30.19), (30.20), (30.21), (30.22), (30.23), (30.24), and (30.25) are negligible compared to the cost required to solve the static load cases in the FEA code. However, larger matrices may exacerbate ill-conditioning in the fitting process leading to less accurate ROMs. Further details on both of the least squares methods can be found in [5].

30.2.3.3 RANSTEP Method

The RANSTEP method determines the nonlinear stiffness coefficients for each modal equation in a series of steps that involve inverting much smaller data matrices. The method solves for the unknown coefficients in sequential steps, beginning with the single-mode displacement fields

$$\begin{aligned} \mathbf{x}_1 &= +\mathbf{T}_i \widehat{q}_i \\ \mathbf{x}_2 &= -\mathbf{T}_i \widehat{q}_i \end{aligned} \tag{30.26}$$

The resulting quasi-static nonlinear modal equations for each mode $r = 1, 2, \ldots, m$ can be written in modal coordinates as

$$\begin{aligned} \mathbf{T}_r^T \mathbf{f}_{T,1} - \mathbf{T}_r^T \mathbf{K} \mathbf{x}_1 &= B_r\,(i,i)\,\widehat{q}_i \widehat{q}_i + A_r\,(i,i,i)\,\widehat{q}_i \widehat{q}_i \widehat{q}_i \\ \mathbf{T}_r^T \mathbf{f}_{T,2} - \mathbf{T}_r^T \mathbf{K} \mathbf{x}_2 &= B_r\,(i,i)\,\widehat{q}_i \widehat{q}_i - A_r\,(i,i,i)\,\widehat{q}_i \widehat{q}_i \widehat{q}_i \end{aligned} \tag{30.27}$$

This relation provides an algebraic equation, similar to the form in Eq. (30.17), as

$$\begin{bmatrix} \widehat{q}_i{}^2\,[1] & \widehat{q}_i{}^3\,[1] \\ \widehat{q}_i{}^2\,[2] & \widehat{q}_i{}^3\,[2] \end{bmatrix} \begin{Bmatrix} B_r\,(i,i) \\ A_r\,(i,i,i) \end{Bmatrix} = \begin{Bmatrix} \mathbf{T}_r^T \mathbf{f}_{T,1} - \mathbf{T}_r^T \mathbf{K} \mathbf{x}_1 \\ \mathbf{T}_r^T \mathbf{f}_{T,2} - \mathbf{T}_r^T \mathbf{K} \mathbf{x}_2 \end{Bmatrix} \tag{30.28}$$

By inverting the 2×2 matrix of modal displacements, the nonlinear stiffness coefficients $B_r(i,i)$ and $A_r(i,i,i)$ can be identified for modes $r = 1, 2, \ldots\ m$ and using all load cases involving modes $i = 1,2, \ldots\ m$.

Similarly, the displacement fields that are combinations of two modes

$$\begin{aligned} \mathbf{x}_1 &= +\mathbf{T}_i \widehat{q}_i + \mathbf{T}_j \widehat{q}_j \\ \mathbf{x}_2 &= -\mathbf{T}_i \widehat{q}_i - \mathbf{T}_j \widehat{q}_j \\ \mathbf{x}_3 &= +\mathbf{T}_i \widehat{q}_i - \mathbf{T}_j \widehat{q}_j \end{aligned} \tag{30.29}$$

and the coefficients from Eq. (30.28) are used to determine the $B_r(i,j)$, $A_r(i,i,j)$, and $A_r(i,j,j)$ coefficients. The displacement fields combining three modes

$$\mathbf{x}_1 = +\mathbf{T}_i \widehat{q}_i + \mathbf{T}_j \widehat{q}_j + \mathbf{T}_k \widehat{q}_k \tag{30.30}$$

are used along with all the other computed nonlinear stiffness terms to compute the $A_r(i,j,k)$ coefficients. Further details can be found in [3].

30.3 Numerical Results: Comparison of Parameter Estimation Method and Scaling Method

The least squares method, both constrained and unconstrained, and the RANSTEP method were first evaluated on a clamped-clamped beam with geometric nonlinearity. The nonlinear beam model, constructed of structural steel, was 228.6 mm (9 in.) long, with a cross section of 12.7 mm (0.5 in.) wide by 0.787 mm (0.031 in.) thick. The material properties are listed below in Table 30.1. The beam was modeled with forty B31 beam elements in Abaqus®, resulting in 117 DOF. In this section, only the axial vibration modes were used to capture the membrane kinematics, as ED ROMs were successfully obtained using these modes on this particular model in [6]. Dual modes are used to model the membrane motions in Sect. 30.4. The ROMs using axial vibration modes were computed with each of the different fitting procedures described in Sect. 30.2.3, along with the two scaling methods in Sect. 30.2.2. The nonlinear normal modes were computed from the reduced equations of motion using the algorithm in [16] and compared to the exact NNMs computed directly from the full FEA model using the AMF algorithm in [17]. The comparison to the full order model allows one to determine at which energy, or response levels, the solutions to the ROM equations deviate from the full model.

Table 30.1 Material properties of clamped-clamped beam

Young's modulus	Shear modulus	Density
$E = 204.8$ GPa (29,700 ksi)	$G = 80.0$ GPa (11,600 ksi)	$\rho = 7{,}870$ kg/m^3 (7.36×10^{-4} lb-s^2/in^4)

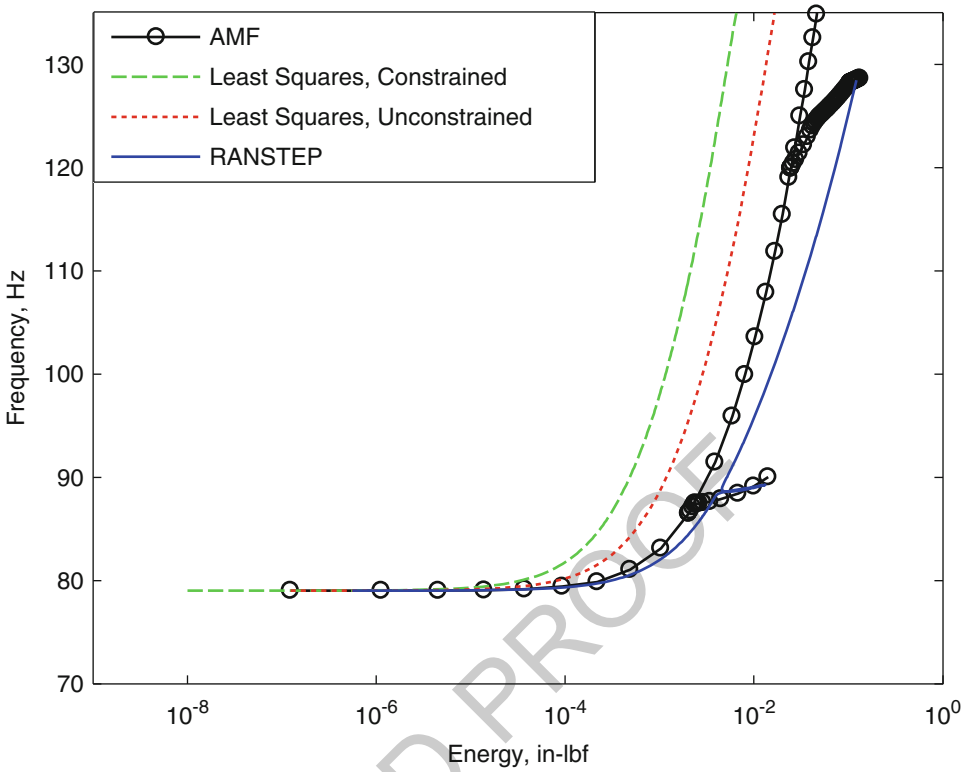

Fig. 30.1 Plot of NNM 1 using modes (1, 3, 5, 7, 26, 39, 45, 47, 49, 51, 53, 55) and a CS scaling set to a maximum displacement of 1.0 times the thickness for mode 1. The (*black circles*) show NNM 1 computed with the AMF algorithm, and ROMs built with the (*green dashed*) least squares constrained method (*red dotted*), least squares method, and (*blue solid*) RANSTEP method

Based on the results from [6], a ROM was successfully computed for the clamped-clamped beam using bending modes 1, 3, 5 and 7, augmented with axial modes 26, 39, 45, 47, 49, 51, 53, 55. The axial modes were chosen based on the static responses discussed in Sect. 30.2.1.1, such that two associated axial modes were added for every bending mode. This basis is used throughout Sect. 30.3 in order to understand how the parameter estimation schemes and scaling factors affect the resulting ROM. The original development of the enforced displacement method by Muravyov and Rizzi suggested using the constant scaling (CS) method to scale each mode during the static displacement fields. The sensitivity of the ED method was observed by using two different CS factors, namely when the first mode was displaced to 3.0 times the beam thickness (referred as CS (3.0)), and 1.0 times the thickness (CS (1.0)). After computing the ROM with these scaling factors, and each of the parameter estimation schemes, the first NNM was computed from the reduced equations and compared to the full order model results (denoted as AMF in the figure legend). These results are presented on the frequency energy plot (FEP) in Figs. 30.1 and 30.2, where the frequency represents the fundamental frequency of the periodic response, and the energy represents the conserved energy (potential plus kinetic) as the structure vibrates in that NNM.

Many interesting observations can be made from these results, and since each ROM used the same basis vectors, the discrepancy can be attributed to the CS scaling level and parameter estimation method. For the smaller CS factor in Fig. 30.1, none of the parameter estimation schemes predicted to correct results. The ROM estimated with RANSTEP was softer than the AMF results, while the two least square methods predicted a stiffer NNM. (Softer or stiffer refers to the fact that at a given energy level the frequency is either lower or higher than the actual frequency, respectively.) These results show that the CS factor of 1.0 is not an adequate scaling factor, even though it was on the order of the beam thickness, as originally recommended.

The results in Fig. 30.2 show the same ROMs but instead with a CS factor set to 3.0 times the beam thickness. At this scaling level, the ROM with RANSTEP produced very accurate results as the first NNM nearly coincides with the AMF results. The ROM with RANSTEP captured solutions along the backbone of the NNM, and also captured the two modal interactions (i.e. the tongues emanating from the backbone around 88 and 120 Hz). Each of the least squares methods were again inaccurate, even though they estimate the nonlinear stiffness coefficients from the same static responses at the same scaling level. Apparently ill-conditioning in the equations leads to higher sensitivity to errors, ultimately producing inaccurate predictions of the NNM. The RANSTEP approach is clearly the favorable method to estimate the nonlinear coefficients, however, one must carefully select the scaling amplitudes to obtain accurate results.

The results in Figs. 30.1 and 30.2 defy the conventional wisdom, which suggests that scaling on the order of the beam thickness will give a valid ROM. The root cause was investigated by computing a single-mode ROM with a particular mode

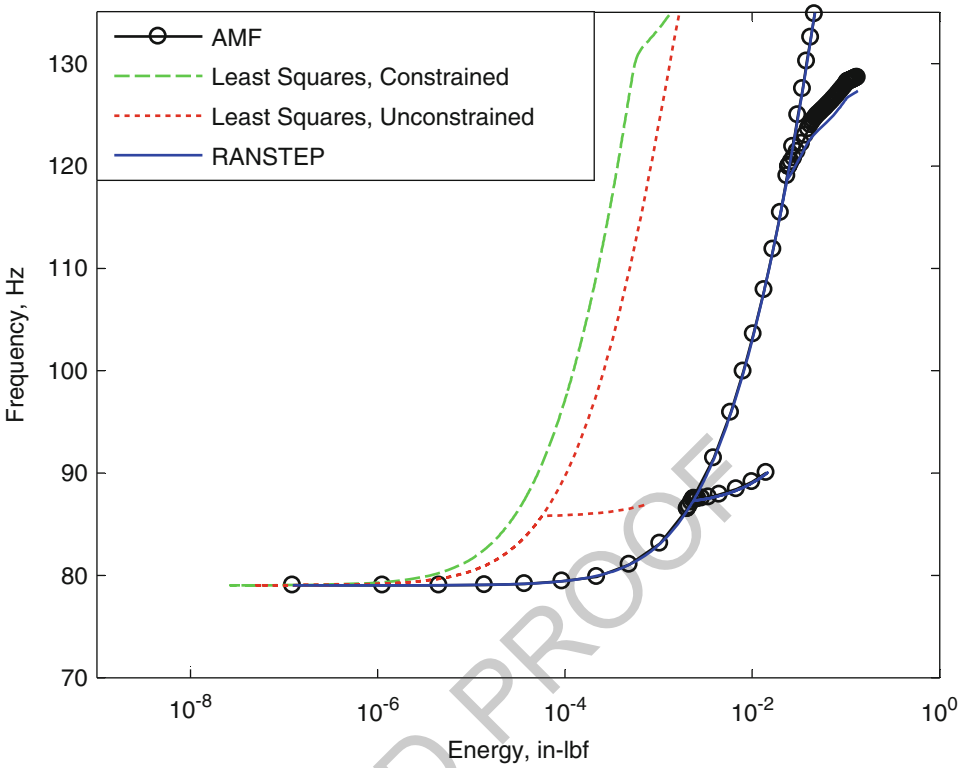

Fig. 30.2 Plot of NNM 1 using modes (1, 3, 5, 7, 26, 39, 45, 47, 49, 51, 53, 55) and a CS scaling set to a maximum displacement of 3.0 times the thickness for mode 1. The (*black circles*) show NNM 1 computed with the AMF algorithm, and ROMs built with the (*green dashed*) least squares constrained method (*red dotted*), least squares method, and (*blue solid*) RANSTEP method

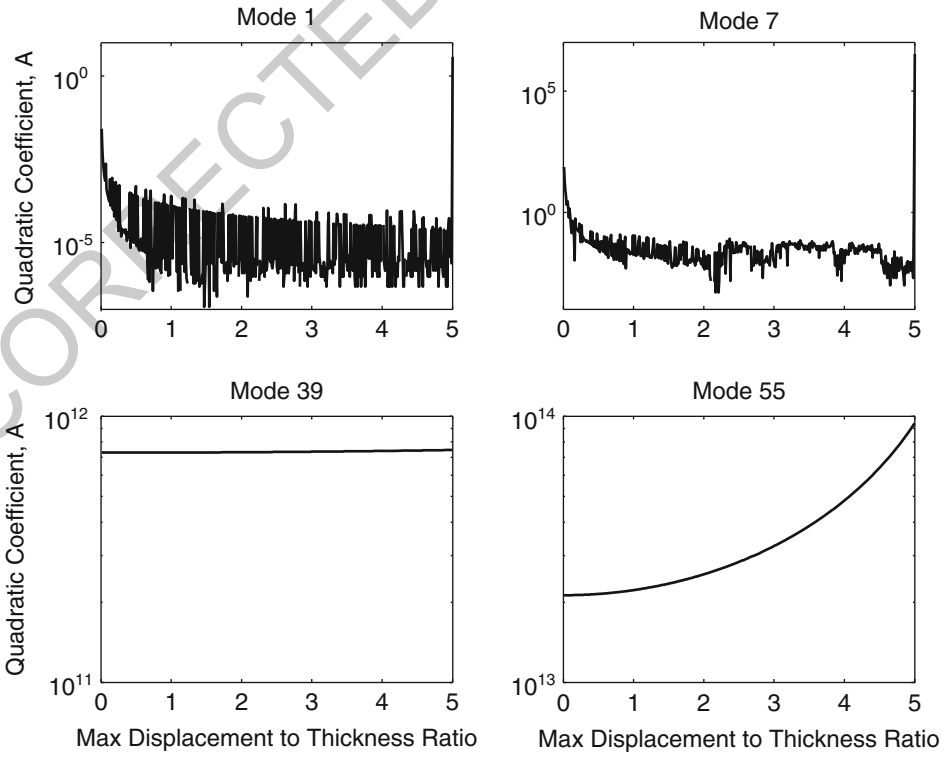

Fig. 30.3 For modes 1, 7, 39 and 55, the effect of scaling is shown for the computed absolute value of the quadratic stiffness term, B1(1,1), of a single-mode ROM

in the basis set, and tracking how the nonlinear quadratic and cubic stiffness coefficients changed with scaling level. Since the difference in the NNM essentially traces back to the stiffness coefficients at the different scaling levels, this provided insight into the scaling range over which each mode could be accurately estimated. Examining a higher and lower mode for both the bending and membrane modes, the absolute values of the stiffness coefficients versus scaling level for bending modes 1 and 7 and membrane modes 39 and 55 are shown in Figs. 30.3 and 30.4.

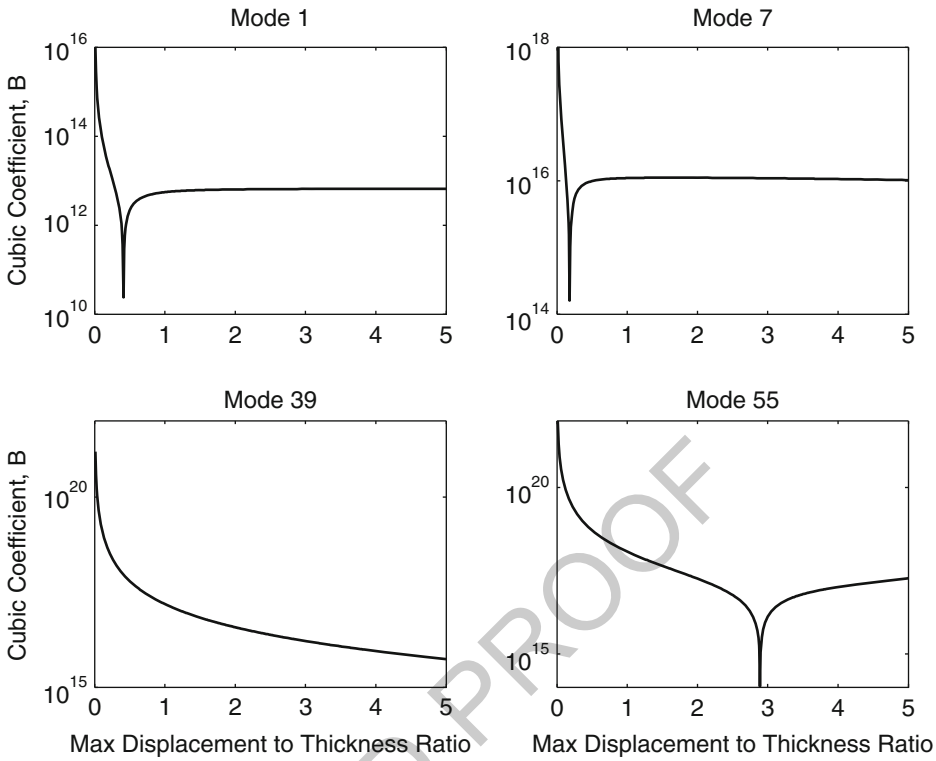

Fig. 30.4 For modes 1, 7, 39 and 55, the effect of scaling is shown for the computed absolute value of the cubic stiffness term, $A_1(1,1,1)$, of a single-mode ROM

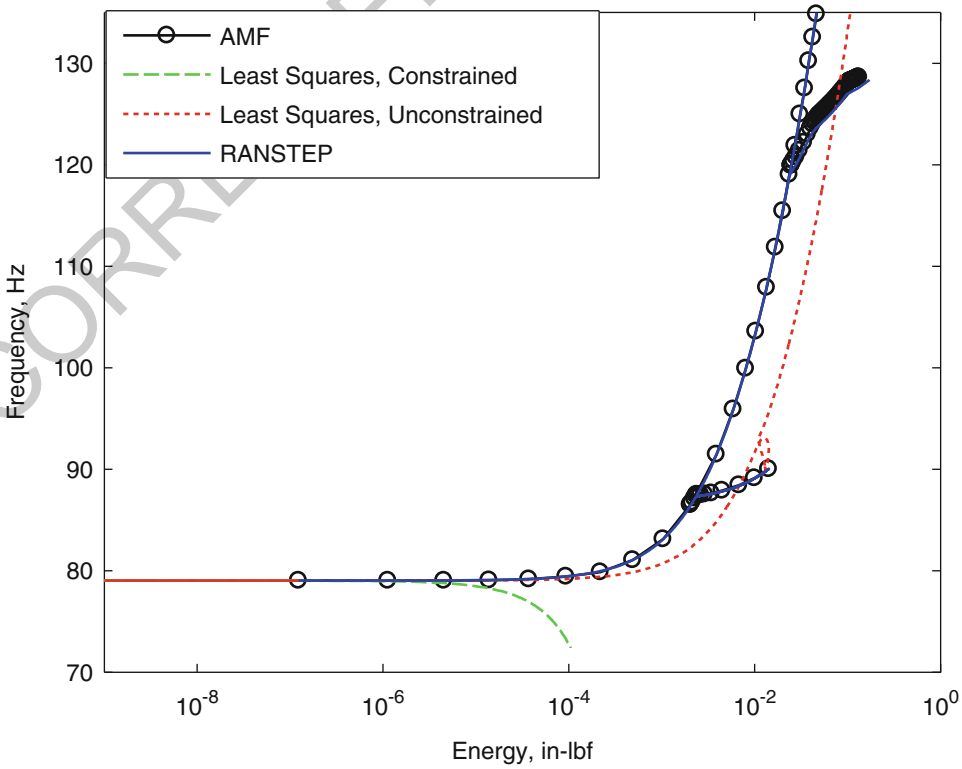

Fig. 30.5 Plot of NNM 1 using modes (1, 3, 5, 7, 26, 39, 45, 47, 49, 51, 53, 55) and a CD scaling set to a maximum displacement of 3.0 times the thickness for all bending modes, and 1.0 times the thickness for all axial modes. The (*black circles*) show NNM 1 computed with the AMF algorithm, and ROMs built with the (*green dashed*) least squares constrained method (*red dotted*), least squares method, and (*blue solid*) RANSTEP method

this figure will be printed in b/w

Table 30.2 Equivalent displacement levels of each mode when using CS set to 3.0 times the thickness

Mode	1	3	5	7	26	39	45	47	49	51	53	55
Equivalent CD levels	3.00	2.85	2.84	2.85	2.67	2.67	2.67	2.54	2.67	2.67	2.67	2.54

For the two bending modes, the quadratic coefficients in Fig. 30.3 were essentially zero, which was expected for the bending modes of a flat structure, but is still informative to see the level of scatter and the regimes where they are estimated to be small. The two axial vibration modes produced quadratic terms that were nonzero. The quadratic term for mode 39 was nearly constant over the entire displacement range, however $B_1(1,1)$ for mode 55 appeared to increase as the scaling increased. The cubic terms were less consistent throughout the scaling range for all of the modes. For both bending modes, the cubic terms were increasing by several orders of magnitude as the displacement tended towards zero. Between displacements of 0 and 1.0 times the beam thickness, the predicted $A_1(1,1,1)$ term dropped down about two orders of magnitude, but began to stabilize as the scaling went above 1.0.

The "bend" of the first NNM predicted in Figs. 30.1 and 30.2 strongly depends on the cubic stiffness coefficient associated with bending mode 1. For mode 1 in Fig. 30.4, scaling of 1.0 times the beam thickness produced a value of $A_1(1,1,1) = 5.52 \cdot 10^{12}$ lbf/in^3, while a scaling of 3.0 produced a value of $6.51 \cdot 10^{12}$ lbf/in^3. The coefficient on mode 1 did not converge until around the range of 2.0 or 3.0 times the beam thickness, which may explain why the scaling of CS (3.0) produced more accurate results than CS (1.0). Unlike the bending modes, the quadratic and cubic terms for the axial modes do not converge within the range of the scaling shown in Figs. 30.3 and 30.4.

The optimal scaling can vary for each mode in the basis, and hence this was the motivation for using the CD scaling method which allows the scaling level to be chosen individually for each mode (recall that the CS method only allows control of the displacement level on the lowest frequency bending mode). New ROMs were again produced using the same basis and parameter estimation schemes, however this time using the CD scaling method. Each of the bending modes was scaled to 3.0 times the beam thickness, while the axial modes were scaled to 1.0 times the beam thickness. Since there was no clear consistency in the coefficients produced by the axial modes in Figs. 30.3 and 30.4, the 1.0 factor was chosen in order to avoid the large spikes in the quadratic or cubic term. The results for NNM 1 are shown in Fig. 30.5.

With the CD scaling method, the ROM with RANSTEP again produced very accurate results, however the least squares methods produced erroneous NNMs. Even though no difference was observed when using the CS or CD scaling with RANSTEP, the CD method provides more flexibility in the selection of scaling each mode during the fitting process. The connection between the CD scaling method, and CS is shown below in Table 30.2, where the equivalent CD factor is given for each mode when using CS (3.0). It can be seen that the displacements on each mode with CS are not drastically different from those used in Fig. 30.5, except that the axial modes are displaced slightly higher (2.5 times the thickness compared to 1.0). The level of the reaction force required to enforce an axial displacement by one thickness tends to be much larger than that required in bending, so the reduced scaling on the axial modes reduced the axial force levels and any associated numerical ill-conditioning, explaining why least squares improved in Fig. 30.5 compared to the results in Fig. 30.2.

30.4 Numerical Results: Axial Modes Versus Dual Modes

The results in Sect. 30.3 showed that the RANSTEP estimation procedure was clearly the preferred method for parameter estimation and that CD scaling was adequate. In this section, the bending modes Eqs. (30.1, 30.3, 30.5, and 30.7) will be used exclusively with RANSTEP and CD in order to evaluate the effect of using dual modes instead of axial modes. The ROMs used in the previous section used 12 modes to capture the response of only four bending modes, so one would hope that a more compact model could be found. Recall from Sect. 30.2.1.2 that three types of dual modes exist, namely generation one, two and three. In the following, a generation one dual mode estimated from bending mode 1 will be referred to as "dual 1" or "D1", and a generation two dual mode with bending modes 1 and 3 will be referred as "dual 1-3" or "D1-3".

Before generating ROMs with the dual mode basis, the appropriate scaling levels for these modes were investigated by computing the single-mode ROMs, and observing how the absolute values of the stiffness coefficients evolved with displacement level. The results for duals 1 and 1–3 are shown in Fig. 30.6.

It was determined that these dual modes should be scaled to 1.0 times the beam thickness when using them to estimate the ROMs, exactly as done with the axial modes in the previous section. There were no large spikes around this value observed in Fig. 30.6 for the dual modes of interest, implying that this would be a safe displacement level to use. The work by Kim et al. [4] discussed the use of dual modes with the enforced displacement procedure, and suggested the use of different

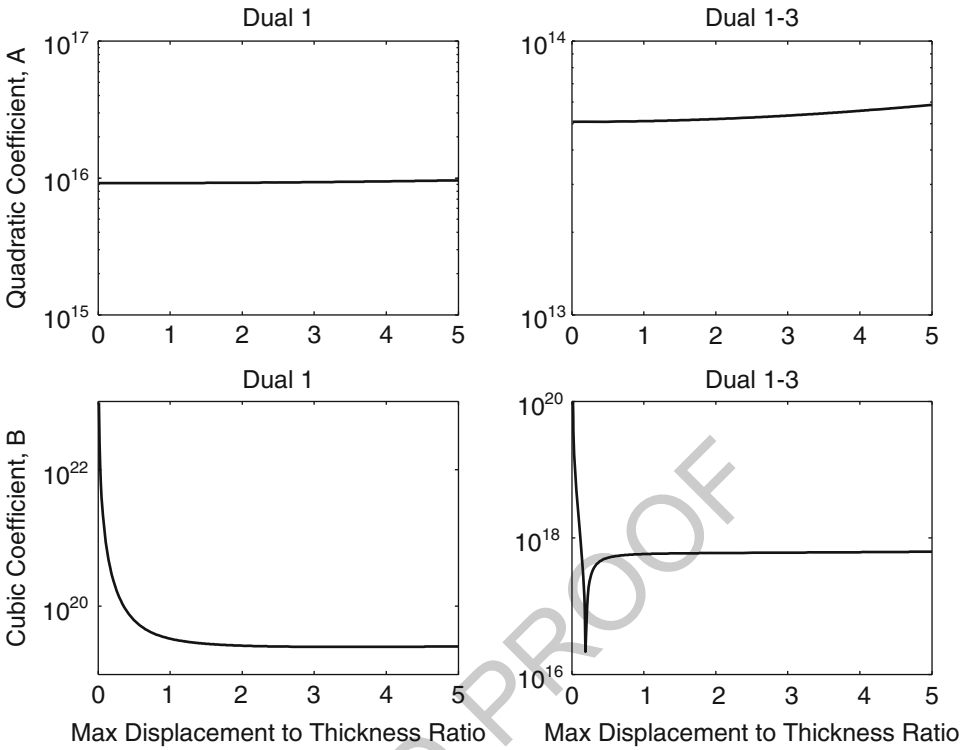

Fig. 30.6 Variation in the absolute values of the cubic and quadratic stiffness terms, $B_1(1,1,1)$ and $A_1(1,1,1)$ for dual modes D1 and D1-3, respectively

Table 30.3 Description of dual mode basis used to generate the ED ROMs

Description	Dual modes included
Generation 1 duals	$\Xi_1^{(1)}, \Xi_3^{(1)}, \Xi_5^{(1)}, \Xi_7^{(1)}$
Generation 1 and 2 duals	$\Xi_1^{(1)}, \Xi_3^{(1)}, \Xi_5^{(1)}, \Xi_7^{(1)}, \Xi_{13}^{(2)}, \Xi_{15}^{(2)}, \Xi_{17}^{(2)}, \Xi_{35}^{(2)}, \Xi_{37}^{(2)}, \Xi_{57}^{(2)}$
Mode 1 dominant duals	$\Xi_1^{(1)}, \Xi_{13}^{(2)}, \Xi_{15}^{(2)}, \Xi_{17}^{(2)}, \Xi_{135}^{(3)}, \Xi_{137}^{(3)}, \Xi_{157}^{(3)}$

combinations of specific dual modes. For example, they discuss using only dual modes computed from one of the dominant bending modes. In the case where bending modes 1, 3, 5, and 7 were used in the basis and mode 1 was expected to be dominant in the responses of interest, then only the dual modes (1, 1-3, 1-5, 1-7, 1-3-5, 1-3-7, 1-5-7) would be included in the ROM. To evaluate the use of dual modes to capture the in-plane kinematics, ROMs were created with only generation one dual modes, generation one and two dual modes, and mode 1 dominant dual modes (see Table 30.3 for a list of dual modes included in each ROM). The resulting ROMs were computed with the RANSTEP method and CD with each bending mode scaled to 3.0 times the thickness and the appropriate duals to 1.0. The ROMs were then compared based on their computed nonlinear normal modes. The results are shown in Fig. 30.7.

The ROM with the mode 1 dominant dual modes (green dashed) performed best when compared to the full order model, as it captured solutions along the backbone as well as the two modal interactions. When using only generation one dual modes (blue solid), the resulting ROM was able to accurately predict solutions along the backbone, but not along the modal interactions. For example, the modal interaction at 88 Hz was an interaction with NNM 3. Since using only generation one dual modes did not include $\Xi_{13}^{(2)}$ or any other higher order dual modes, the necessary kinematics were not available in the ROM to fully capture this interaction. When using generation one and two dual modes (red dotted), the ROM was able to capture this interaction, further implying that the higher order kinematics were important.

There was one additional challenge with the ROM that was built with generation one and two dual modes; the authors were not able to compute NNM solutions beyond 100 Hz with this ROM. (Notice that the red dotted line in Fig. 30.7 does not continue past this point.) A similar observation was made when a ROM was constructed including all of generation one, two, and three dual modes (not shown here). With this ROM the continuation algorithm could not compute past the linear range of the NNM so its NNM was not included in Fig. 30.7. Apparently some of these higher generation modes introduce some instability in the ROM equations at certain amplitude levels. One would hope that adding additional basis vectors to the ROM would improve the results, or at the very least have no ill effect on the results so this behavior is certainly undesirable. The cleaning procedure [15] briefly mentioned in Sect. 30.2.2 would perhaps help with this issue, although it was not explored in this paper.

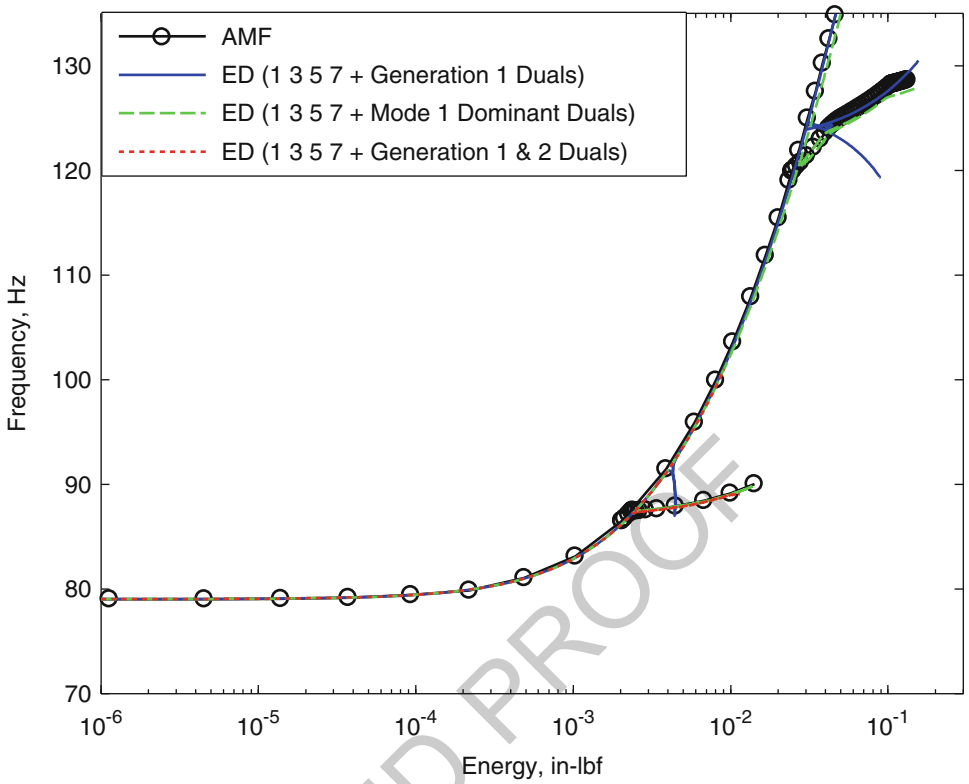

Fig. 30.7 Plot of NNM 1 using bending modes (1, 3, 5, 7) and various combinations of dual modes. A CD scaling factor was set to a maximum displacement of 3.0 times the thickness for all bending modes, and 1.0 times the thickness for all dual modes. The (*black circles*) show NNM 1 computed with the AMF algorithm, and ROMs built with the (*blue solid*) generation 1 dual modes (*green dashed*), mode 1 dominant dual modes, and (*red dotted*) generation 1 and 2 dual modes

30.5 Numerical Results: FEA Model of Exhaust Cover Plate

A more complicated model is used now to evaluate the ability of the enforced displacement ROMs to accurately predict NNMs of a structure for which an analytical solution is intractable. The FEA model of interest is a perforated exhaust cover plate and is shown in Fig. 30.8. A similar model was studied in [6, 17], but the model here has an improved mesh. When the authors originally investigated this model, they found that it was difficult to identify axial modes to augment the bending modes and hence an accurate ROM was not obtained in [6]. Here, the problem is revisited in an attempt to model the in-plane kinematics with dual modes.

The exhaust cover plate is 317.5 mm (12.5 in.) in diameter with a uniform thickness of 1.5 mm (0.059 in.). It is constructed of structural steel with a mass density of 7,800 kg/m^3 (7.29 · 10-4 lb-s^2/in^4) and a Young's modulus of 208 GPa (30,160 ksi). The Abaqus® model has a total of 1,440 S4 shell elements, and a total of 8,886 DOF. The boundary conditions were approximated as fixed along the bottom ring of the plate in order to account for the relatively rigid boundary to which the plate is welded.

The first NNM of the nonlinear plate model was computed using the AMF algorithm, and used to compare five different ROMs. Four of the ROMs used bending modes (1 and 6), and "axial" modes (126, 135, 142, 157, 169, 375). These "axial" modes were selected based on the static displacement results in Sect. 30.2.1.1, however each selected mode shape still had noticeable transverse deformation and no true in-plane modes were identified. Another ROM was created with the same bending modes, but instead with all the first and second generation dual modes ($\Xi_1^{(1)}$, $\Xi_6^{(1)}$, $\Xi_{16}^{(2)}$). For all cases, the RANSTEP parameter estimation procedure was used, and the CD scaling factors were selected such that the bending modes and membrane (axial or dual) modes were displaced between 0.5 and 3.0 times the plate thickness. The frequency-energy behavior of the NNMs estimated from these ROMs are shown in Fig. 30.9.

The enforced displacement ROMs that were built with axial modes and scaled the bending modes to a maximum displacement of 3.0 times the thickness predicted stiffer NNMs than the full order model, as expected from previous works [6]. The ROM that was built with axial modes and scaled the bending and membrane modes to a maximum displacement of 1.0 times the thickness predicted slightly stiffer behavior at lower energies and then slightly softer behavior at higher energies. For any of these first three ROMs with axial modes in the legend of Fig. 30.9, the accuracy may be acceptable for some purposes. However, the last ROM created with axial modes predicted unphysical behavior, likely due to the low scaling factors used during the static loads to fit the nonlinear coefficients. Additional kinematics are needed to

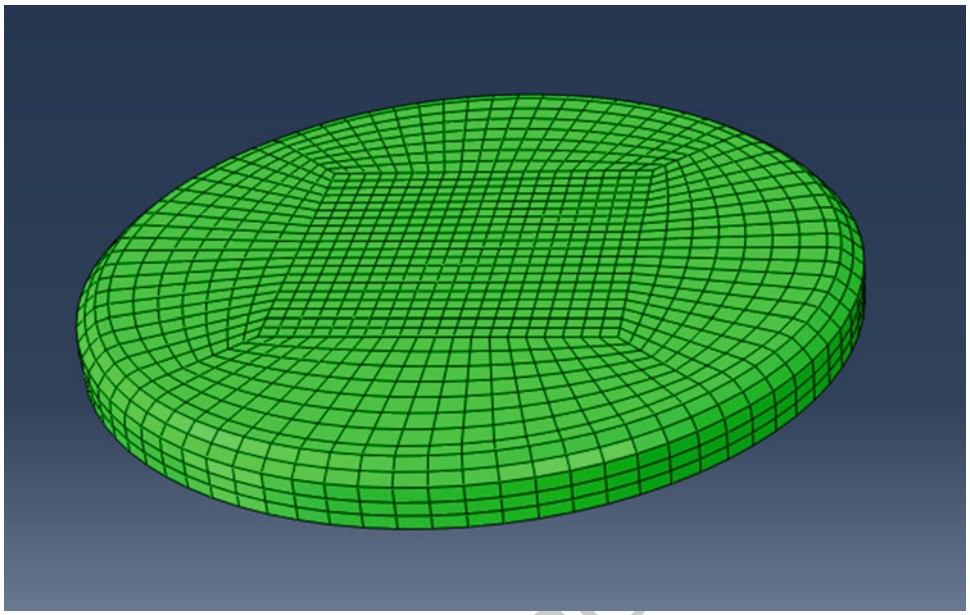

Fig. 30.8 A geometrically nonlinear finite element model of an exhaust cover panel

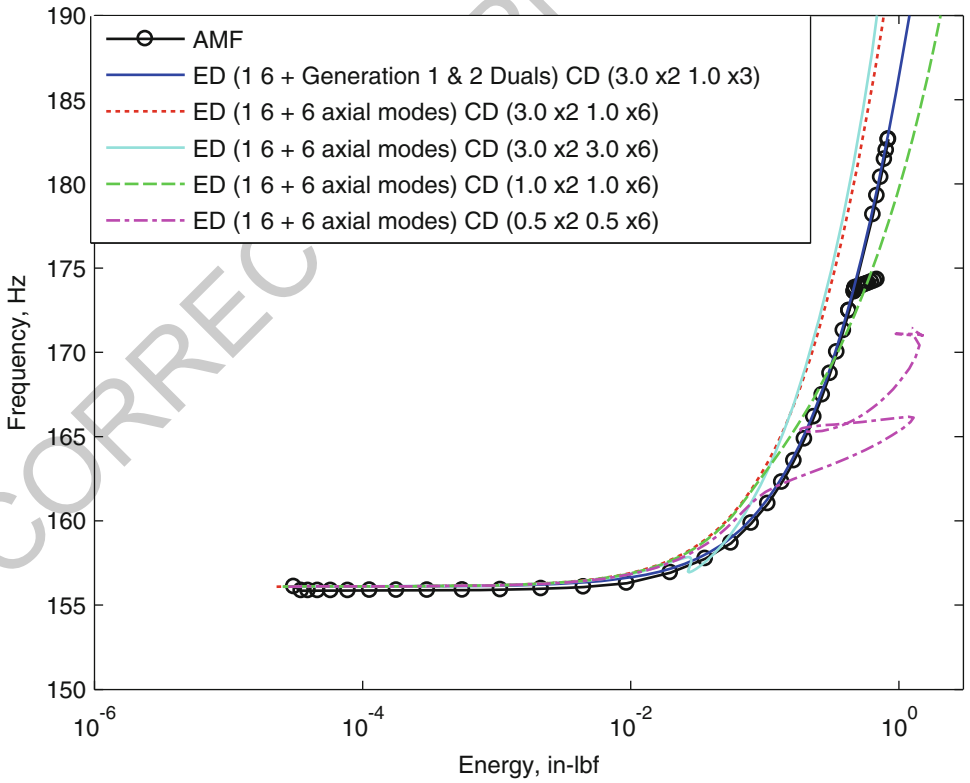

Fig. 30.9 Plot of NNM 1 using bending modes (1 and 6) with either all generation one and two dual modes ($\Xi_1^{(1)}$, $\Xi_6^{(1)}$, $\Xi_{16}^{(2)}$), or six axial modes (126, 135, 142, 157, 169, 375). Various values for the CD scaling factors were used for the bending and membrane modes and the parameters were fit with RANSTEP. The (*black circles*) show NNM 1 computed with the AMF algorithm

improve the accuracy of this model when using axial modes, but it is difficult to determine which modes are needed. Plus, the model already has three times as many axial modes as it does bending modes, so additional modes increase the cost required to build the ROM. The ROM with dual modes worked very well as the predicted backbone coincided with the AMF results almost perfectly. This ROM was not able to capture the modal interaction near 175 Hz, however this is to be expected because this internal resonance was an interaction with NNM 15, a bending motion that was not included in the basis set. The use of dual modes provided a systematic approach to model the in-plane deformations, with only 3 in-plane component mode shapes, and provided very accurate results for the exhaust cover plate model.

30.6 Conclusion

This work has explored the effect of the various decisions to generate a ROM using the enforced displacement procedure by comparing the accuracy of its computed nonlinear normal modes. The results in Sect. 30.3 clearly showed that the RANSTEP procedure was much more robust at estimating the coefficients in the reduced order models than the least squares procedure. This may also suggest that one can expect RANSTEP to be less sensitive to the amplitude of the load cases than the least squares approach. The effect of the scaling of the modal displacements on these ROMs was also investigated. So long as RANSTEP was used, either scaling method was found to be accurate as long as the bending modes were displaced a few times the beam thickness. Previous works have made general recommendations of using a displacement on the order of the thickness [3]. However, this discrepancy could be attributed to the fact that we assumed the linear term on the ROM equation was determined from an eigenvalues solution, whereas in the works by Perez, they fit this when fitting the nonlinear terms. The CD scaling method is recommended based on the flexibility it allows to displace each mode in the basis set.

This work has also explored the number of axial or dual modes that are needed to obtain an accurate ROM. For the systems studied here it was sometimes possible to obtain an accurate ROM by simply selecting those axial modes that were statically coupled to each of the bending modes in the basis. This worked for the beam but the ROM for the exhaust plate seemed to converge slowly to the true NNM and there was noticeable inaccuracy even after several axial modes had been included. In contrast, when dual modes were used, an accurate ROM for the exhaust plate was obtained with only two bending modes and three dual modes. For the beam, the dual modes consistently produced ROMs that accurately captured the backbone of the NNM. However, only the ROM with mode 1 dominant duals captured the internal resonances correctly. Additionally, several of the ROMs with dual modes could not be integrated at large response amplitudes, presumably due to small errors in some of the nonlinear coefficients. It was noted that Mignolet, Perez and Wang [2, 7, 8, 15] typically use the cleaning procedure in the papers just cited to set certain terms in the ROM to zero. Perhaps this is a critical step when using these methods. However, it is important to note that cleaning can only be done when the structure is flat since one needs to be able to classify each mode as either axial or bending. For a curved structure, all modes contain bending and membrane components, making it difficult to apply this approach.

In summary, the results so far confirm the effectiveness of the enforced displacements procedure so long as the best practices outlined above are used. It seems to exhibit some sensitivity to the displacement levels but these can be addressed by computing single-mode ROMs at different scaling levels and seeing how the coefficients change. These ROMs tend to produce larger reduced order models since the membrane modes need to be explicitly included in the basis, and these can be hard to identify. Dual modes seem to be promising as a means of obtaining an efficient ROM with relatively few membrane degrees of freedom, but some expertise is still required to choose a set of dual modes that will be accurate while keeping the ROM small.

Acknowledgements The authors gratefully acknowledge the support of the Air Force Office of Scientific Research under grant number FA9550-11-1-0035, administered by Dr. David Stargel of the Multi-Scale Structural Mechanics and Prognosis Program. The authors also wish to thank Dr. Joseph Hollkamp and the Structural Sciences Center at the Air Force Research Laboratory for providing the Abaqus® interface that was used in this work as well as for many helpful suggestions and discussions regarding the ROM modeling and Dr. Stephen Rizzi for providing an implementation of the RANSTEP code and suggestions regarding how to use it effectively. The authors are also grateful to Ricardo Perez (Universal Technologies Inc. and AFRL) for his insights and comments regarding how to create accurate ROMs.

References

1. Hollkamp JJ, Gordon RW, Spottswood SM (2005) Nonlinear modal models for sonic fatigue response prediction: a comparison of methods. J Sound Vib 284:1145–1163
2. Mignolet MP, Przekop A, Rizzi SA, Spottswood SM (2013) A review of indirect/non-intrusive reduced order modeling of nonlinear geometric structures. J Sound Vib 332:2437–2460
3. Muravyov AA, Rizzi SA (2003) Determination of nonlinear stiffness with application to random vibration of geometrically nonlinear structures. Comput Struct 81:1513–1523
4. Kim K, Radu AG, Wang XQ, Mignolet MP (2013) Nonlinear reduced order modeling of isotropic and functionally graded plates. Int J Non-Lin Mech 49:100–110
5. Gordon RW, Hollkamp JJ (2011) Reduced-order models for acoustic response prediction. AFRL-RB-WP-TR-2011-3040, July 2011
6. Kuether RJ, Deaner BJ, Hollkamp JJ, Allen MS (2014) Evaluation of geometrically nonlinear reduced order models with nonlinear normal modes. AIAA J (submitted)
7. Perez R, Wang XQ, Mignolet MP (2014) Nonintrusive structural dynamic reduced order modeling for large deformations: enhancements for complex structures. J Comput Nonlin Dyn 9:031008–031008

AQ1

8. Perez RA (2012) Multiscale reduced order models for the geometrically nonlinear response of complex structures. PhD, Arizona State University
9. Rizzi SA, Przekop A (2005) The effect of basis selection on static and random acoustic response prediction using a nonlinear modal simulation. NASA TP-2005-213943
10. Kerschen G, Peeters M, Golinval JC, Vakakis AF (2009) Nonlinear normal modes. Part I. A useful framework for the structural dynamicist. Mech Syst Signal Process 23:170–194
11. Vakakis AF (1997) Non-linear normal modes (NNMs) and their applications in vibration theory: an overview. Mech Syst Signal Process 11:3–22
12. Kuether RJ, Brake MR, Allen MS (2014) Evaluating convergence of reduced order models using nonlinear normal modes. Presented at the 32nd international modal analysis conference (IMAC XXXII), Orlando
13. Schoneman JD, Allen MS, Kuether RJ (2014) Relationships between nonlinear normal modes and response to random inputs. Presented at the 5th AIAA/ASME/ASCE/AHS/SC structures, structural dynamics, and materials conference, National Harbor
14. Rizzi SA, Przekop A (2008) System identification-guided basis selection for reduced-order nonlinear response analysis. J Sound Vib 315:467–485
15. Wang XQ, Perez RA, Mignolet MP, Capillon R, Soize C (2013) Nonlinear reduced order modeling of complex wing models. In: 54th AIAA/ASME/ASCE/AHS/ASC structures, structural dynamics, and materials conference, Boston
16. Peeters M, Viguié R, Sérandour G, Kerschen G, Golinval JC (2009) Nonlinear normal modes, Part II: toward a practical computation using numerical continuation techniques. Mech Syst Signal Process 23:195–216
17. Kuether RJ, Allen MS (2014) A numerical approach to directly compute nonlinear normal modes of geometrically nonlinear finite element models. Mech Syst Signal Process 46:1–15

AUTHOR QUERY

AQ1. Please provide volume and page range for Ref. [9].